Available online at www.sciencedirect.com

ScienceDirect

Acta Materialia 63 (2014) 63–72

Acta MATERIALIA

www.elsevier.com/locate/actamat

# Investigation of secondary hardening in Co–35Ni–20Cr–10Mo alloy using analytical scanning transmission electron microscopy

D. Sorensen [a,b], B.Q. Li [a], W.W. Gerberich [b], K.A. Mkhoyan [b,*]

[a] Medtronic Neuromodulation, Fridley, MN 55432, USA

[b] Department of Chemical Engineering and Materials Science, University of Minnesota, Minneapolis, MN 55455, USA

Received 7 June 2013; received in revised form 2 October 2013; accepted 4 October 2013
Available online 6 November 2013

**Abstract**

The mechanism of secondary hardening in MP35N (Co–35Ni–20Cr–10Mo) alloy due to exposures at elevated temperatures has been studied. It was observed that short exposure to elevated temperatures increased the ultimate tensile strength and yield stress while decreasing the elongation of MP35N wires. Upon aging at temperatures from 300 to 900 °C the elastic modulus increased although no changes in crystallographic orientation or microstructure were observed. The grain size and major texture components were unchanged following aging. Analytical scanning transmission electron microscope investigation showed that MP35N is hardened by preferential segregation of molybdenum to stacking faults and deformation twins. It also revealed that the concentration of molybdenum segregation was proportional to the amount of initial cold work before aging.


*Keywords:* Secondary hardening; Aging; MP35N; STEM; EELS

## 1. Introduction

MP35N (Co–35Ni–20Cr–10Mo) is a Co-based superalloy developed as a family of Co–Ni-based alloys in 1968 by Smith [1] as part of a family of single-phase γ Co-based alloys that are commonly used in the medical device industry. High strength, fatigue and corrosion resistance, and biocompatibility [2–4] make MP35N an ideal material for conductor coils and cables in cardiac pacing and neurostimulation leads. For medical device applications, MP35N wires go through numerous processing steps starting from cold-drawn wire. The majority of secondary and tertiary manufacturing processes, including polymer insulation coating, wire coiling and cabling occur at elevated temperatures for durations of seconds to minutes. These high-temperature exposures have significant effects on the mechanical and elastic properties of MP35N wire.

Shortly after the development of MP35N it was discovered that cold work increased the yield strength of this alloy by up to a factor of five. Initial studies suggested that this is due to the presence of thin platelets with a hexagonal structure [5]. Electron diffraction experiments suggested that the platelets should have an orientation relationship with the matrix of $\{111\}_{fcc}\|\{0001\}_{hcp}$ and $[1\,10]_{fcc}\|\{11\bar{2}0\}_{hcp}$ [5]. Since multiphase alloys with Co:Ni ratios greater than 45:25 were reported to strengthen the material by the formation of stress-induced hexagonal martensite (ε phase) plates [5–7], formation of hexagonal platelets in MP35N is somewhat expected. However, further investigations showed the platelets formed following plastic deformation in MP35N to be deformation twins [7]. While there are some reports on the strengthening mechanism of MP35N following aging, the conclusions have been controversial with hypotheses ranging from precipitation of $Co_3Mo$ phase [6], solute partitioning to hexagonal close-packed (hcp) martensite plates [8], to segregation of solute atoms to stacking faults and the nucleation and growth of hcp martensite [9]. More recent studies also suggested that

* Corresponding author. Tel.: +1 612 625 2059; fax: +1 612 626 7246.
*E-mail addresses:* dan.sorensen@medtronic.com (D. Sorensen), mkhoyan@umn.edu (K.A. Mkhoyan).

1359-6454/$36.00 
http://dx.doi.org/10.1016/j.actamat.2013.10.005

the plate-like features in MP35N are deformation twins and stacking faults [10–12] and not hcp phases.

Here we present a detailed experimental study using a variety of analytical techniques, including atomic-resolution imaging and spectroscopy, showing how the mechanical properties of MP35N rod and fine wire can be changed by brief exposures to elevated temperatures. The mechanisms for the observed changes are also discussed. It was observed that Mo segregates at stacking faults and twins when MP35N is exposed to elevated temperatures. The finding is correlated with mechanical test data showing that the material strengthens and the elastic modulus increases upon aging.

## 2. Experimental

MP35N rod and wire samples were obtained from Accellent (Salem, PA) and Fort Wayne Metals (Fort Wayne, IN) with varying amounts of prior cold work. Table 1 lists the samples used for this study and their sample designations. The chemical composition of each sample is given in Table 2.

All aging treatments of the samples were performed using a muffle furnace in an air atmosphere. Samples of rodstock were aged at 600 °C for 30 min. Wire samples were heat treated at temperatures ranging from 300 to 1000 °C for 60 s. Following the aging treatment the samples were removed from the furnace and allowed to cool in air. The aging time and temperatures were chosen to represent fine wire processing parameters or were based on results of previous reports [9].

Wire samples were cut to 30.5 cm lengths and tension tested using an MTS QTest 5 load frame with a 250 N load cell. Strain was measured using an MTS LX500 laser extensometer. All samples were pulled with a 25.4 cm gage length with a crosshead speed of 0.02 cm $s^{-1}$.

Electron backscatter diffraction (EBSD) experiments were performed on a Zeiss Ultra Plus field emission scanning electron microscope equipped with an EDAX OIM system for analysis. EBSD experiments were performed on three separate wire sections from each heat-treatment and cold-work condition to ensure a statistical sampling. EBSD specimens were prepared by mounting specimens in the transverse direction using ProbeMet conductive mounting compound. All samples were mechanically polished using a Buehler EcoMet/AutoMet 250 polisher followed by a vibratory polish using a Buehler Vibromet 2 polisher to remove any residual surface strains [13].

Conventional and analytical transmission electron microscopy (TEM) was performed using an FEI Tecnai $G^2$ F30 Schottky field-emission gun microscope operating at 300 kV, equipped with an EDAX X-ray detector and a Gatan electron energy loss spectrometer [14]. TEM samples from the wires were prepared using both FEI Versa and FEI Quanta 3D dual-beam focused ion beam millers equipped with an in situ Omniprobe micro-manipulator for lift out. Samples from rods were prepared by twin-jet electropolishing (using a Fischione model 110 twin-jet electropolisher) at 10 V and 25 °C after being machined to 2.9 mm diameter rods from which 150 μm thick disks were cut (using a Buehler IsoMet Low Speed precision saw) that were ground to thicknesses ranging from 60 to 80 μm.

Table 1
Materials used in this study.

| Sample | Form (diameter) | Prior cold work (%) | Supplier |
|---|---|---|---|
| A | Wire (178 μm) | 37 | Fort Wayne Metals |
| B | Wire (178 μm) | 60 | Fort Wayne Metals |
| C | Rod (3 mm) | 25 | Accellent |
| D | Rod (3 mm) | 48 | Accellent |

## 3. Results

### 3.1. Mechanical testing

The results of the uniaxial tension tests on as-drawn and aged MP35N wires, presented in Fig. 1a, showed a visible increase in yield strength with an increase of aging temperature. Both sample A with 37% and sample B with 60% cold work, aged at 700 °C, reached the maximum yield strengths of about 2045 and 2602 MPa, respectively. However, when the aging temperature was increased above 700 °C, a rapid decrease in yield strengths was also observed. The values of the fracture strain were also measured for these aging conditions (Fig. 1b), and were found to decrease as the aging temperature increased. Interestingly, the elongation in 37% and 60% cold-worked wires continued decreasing even when yield stress began to decrease at aging temperatures above 700 °C.

For these tensile experiments, reduction in area (RA) measurements were also conducted. Figs. 2 and 3 show representative SEM images of fractured wires, and a summary of the RA values is shown in Fig. 4. Wires of sample A (37% prior cold work) were found to have an average RA value of about 42% in the as-drawn condition. For this sample, as the aging temperature increased, average RA

Table 2
Elemental composition of the MP35N samples listed in Table 1.

| Sample | Ni | Cr | Mo | Ti | C | S | P | B | Mn | Si | Fe |
|---|---|---|---|---|---|---|---|---|---|---|---|
| A | 35.9 | 19.72 | 10.21 | <0.005 | 0.0115 | <0.0023 | <0.005 | 0.016 | 0.020 | 0.075 | 0.080 |
| B | 35.88 | 19.57 | 10.14 | 0.018 | 0.0160 | 0.0025 | <0.005 | 0.005 | <0.005 | 0.076 | 0.083 |
| C and D | 34.9 | 20.56 | 9.47 | 0.69 | 0.009 | 0.001 | 0.002 | 0.010 | 0.01 | 0.01 | 0.23 |

The values are in wt.%. The balance is Co.

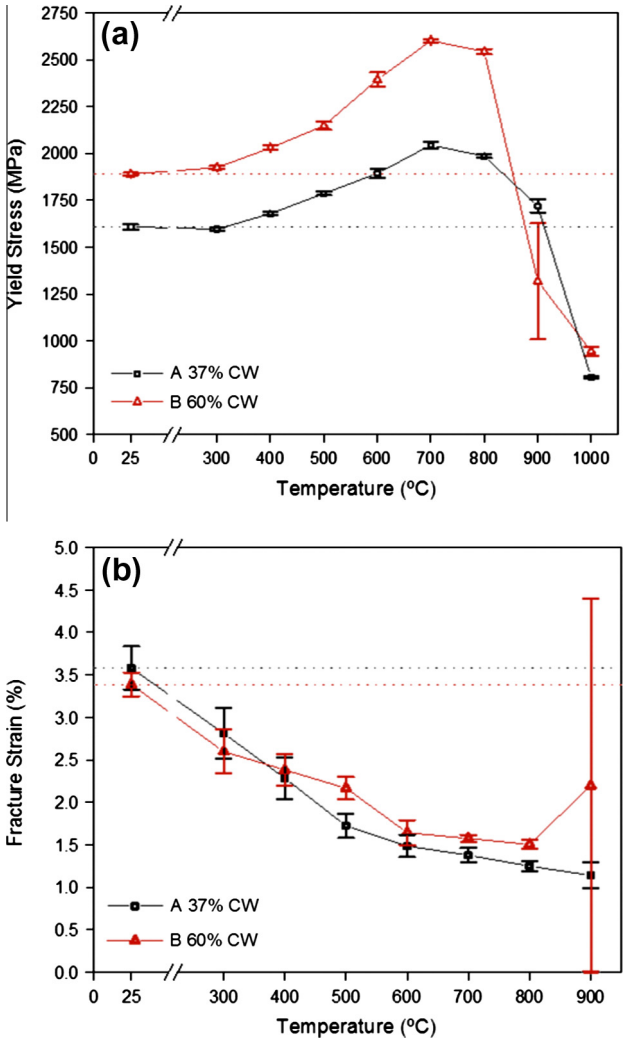


Fig. 1. (a) 0.2% Offset yield stress and (b) strain at fracture as a function of aging temperature and prior cold work in wire samples A and B. The samples were aged for 60 s. The error bars correspond to a 95% confidence interval.

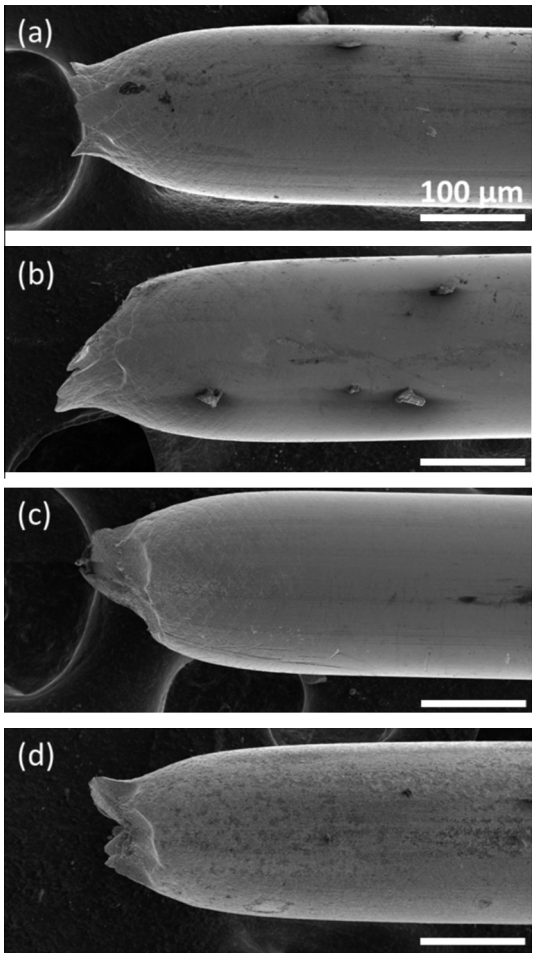


Fig. 2. SEM images of fractured MP35N wires from sample A (37% prior cold work) following various thermal treatments: (a) as drawn; (b) 500 °C for 60 s; (c) 700 °C for 60 s; (d) 900 °C for 60 s.

values decreased with a minimum average of 26% following aging at 900 °C. Wires of sample B (60% cold work) with 31% RA prior to aging, responded to the thermal treatments differently. The RA values in these wires fell to 1% after aging at 700 °C and recovered at higher temperatures. The onset of recovery and recrystallization caused the RA values to increase at the higher temperatures. These RA measurements are consistent with previous studies both on fine wires aged for short times [15] and on highly cold worked and large-diameter MP35N bars aged at 593 °C for 4 h [16]. Research by Drapier et al. [6] indicated that bulk MP35N samples with similar temperature exposures may require many hours before a large ductility loss can be observed.

The elastic moduli for both samples A and B were also measured as a function of aging temperature and prior cold work. The results, presented in Fig. 5, show unusual behavior. Drawing fine MP35N wires resulted in a decrease in elastic modulus. The decrease in Young's modulus was of the order of 59–64 GPa between fully annealed and cold-worked MP35N wire. Following 60 s exposures to elevated temperatures the elastic modulus began to recover until the microstructure was fully recrystallized and the elastic modulus reached the commonly reported values of about 230 GPa [17,18]. The change in elastic modulus can be attributed to dislocations introduced during cold work that become pinned and bowed by solute atoms as suggested by Benito et al. [19].

The maximum increases in the yield strength, ultimate tensile strength and elastic modulus, and decreases in the maximum elongation for these wires are summarized in Table 3.

### 3.2. Electron backscatter diffraction measurements

Studies by Li et al. [20] showed that the mechanical and elastic properties of MP35N can be highly anisotropic and the texture of MP35N wires was found to have a significant effect on the modulus of elasticity and fatigue performance of the wires. EBSD was used in this study to characterize the preferred crystallographic orientations and to measure

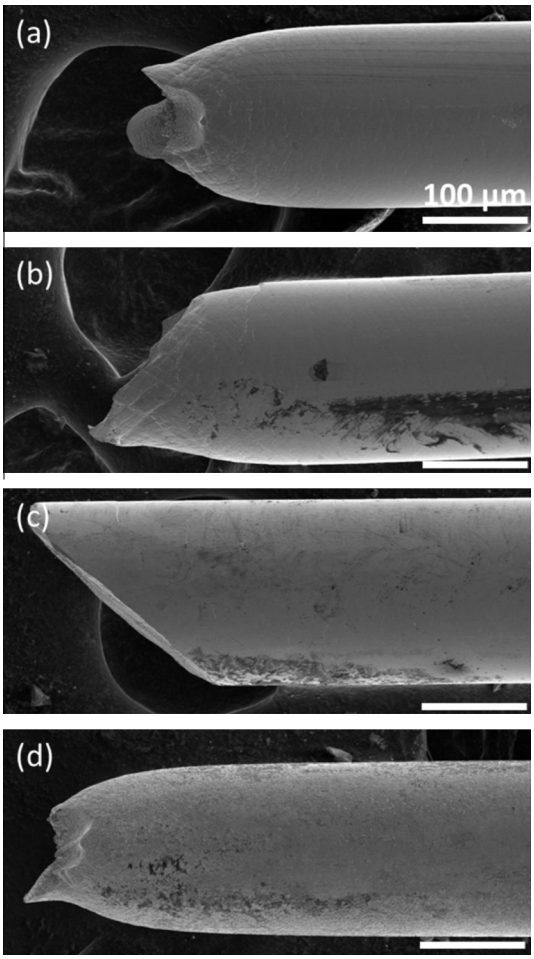


Fig. 3. SEM images of fractured MP35N wires from sample B (60% prior cold work) following various thermal treatments: (a) as drawn; (b) 500 °C for 60 s; (c) 700 °C for 60 s; (d) 900 °C for 60 s.

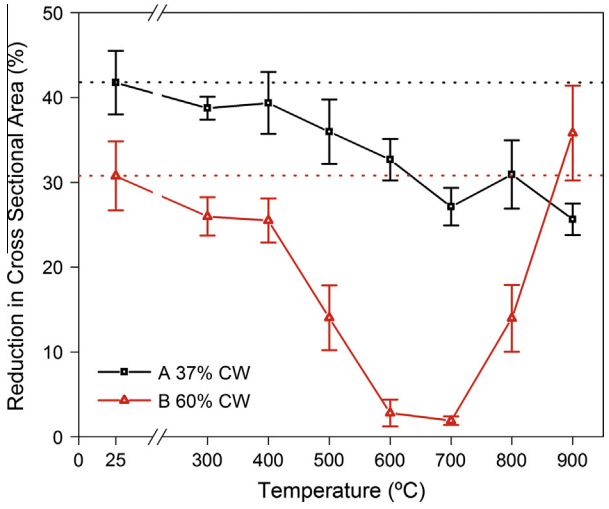


Fig. 4. RA measurements of samples A and B as a function of aging temperature. The samples were aged for 60 s. The error bars correspond to a 95% confidence level.

the grain sizes of the MP35N wires following thermal treatments. Representative image qualities (IQs) with overlaid orientation image maps (OIMs) and corresponding pole

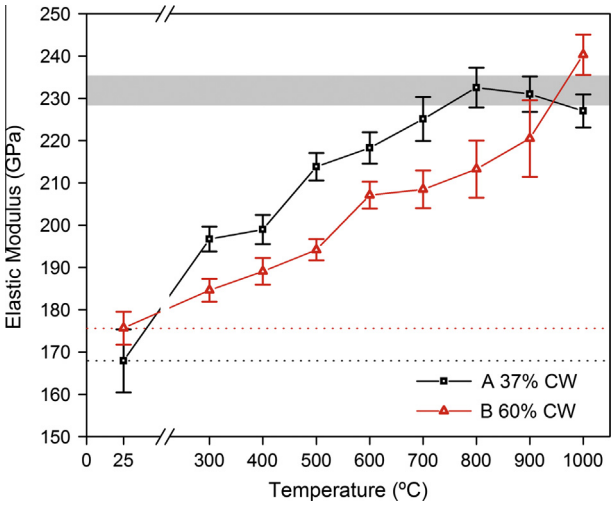


Fig. 5. Elastic modulus of MP35N wires (samples A and B) measured as a function of aging temperature. The shaded gray region indicates the range of reported elastic modulus values for fully annealed MP35N sample [16,17]. The error bars correspond to a 95% confidence level.

figures recorded from wires cold-drawn and wires cold-drawn and aged at 700 °C for 60 s are shown in Fig. 6.

The analysis of the area fractions of the ⟨1 1 1⟩ and ⟨0 0 1⟩ texture components is shown in Fig. 7. As can be seen, aging of MP35N wires does not alter the area fractions of the main texture components until the wires were exposed to temperatures of 900 °C or above. These results indicate that the changes in mechanical properties or elastic modulus upon aging were probably not related to a texturing of the material. The OIM analysis also shows that, compared to wires with 37% prior cold work, the wires with 60% prior cold work have a considerably higher area fraction of [1 0 0] oriented grains. The differences in elastic moduli in samples A and B, seen in Fig. 5, can be due to differences in sample texturing. MP35N specimens with a heavy [1 0 0] texture have been found to have a lower elastic modulus compared to those with a strong [1 1 1] texture [20].

The average grain size was found to be 1.6 and 1.0 μm for cold-drawn wire samples A and B, respectively. The grain size remained consistent following aging treatments up to 1000 °C, as shown in Fig. 8.

### 3.3. Conventional and analytical transmission electron microscopy

To better characterize the effect of thermal treatments on MP35N wires and determine whether the changes in mechanical properties are result of microstructural changes, wires of sample A aged at 700 °C for 60 s and 900 °C for 60 s were investigated using TEM. Bright-field and dark-field (BF/DF) imaging and selected-area diffraction (SAD) analysis did not show the presence of any non-face-centered cubic (fcc) phases. However, deformation twins and stacking faults were observed in both samples. The concentrations and distribution of the

Table 3
Maximum changes in mechanical properties of aged MP35N wires.

| | Δ Tensile strength (%) | Δ Yield stress (%) | Δ Elongation (%) | Δ Elastic modulus (%) |
|---|---|---|---|---|
| 37% | +15 | +21 | −68 | +28 |
| 60% | +18 | +27 | −53 | +27 |

deformation twins and faults remained unchanged after aging. Fig. 9 shows representative images of deformation twins found in sample A following a thermal treatment at 700 °C for 60 s.

Samples of the aged MP35N rods were also analyzed for microstructural changes and for possible formation of second phases after exposure to elevated temperatures. TEM imaging and SAD analysis of as-drawn MP35N rods of samples C and D (25% and 48% prior cold work, respectively) showed again a microstructure consisting of deformation twins and stacking faults along {1 1 1} habit planes within a fcc matrix (Fig. 10). No microstructural changes were observed after aging below the recrystallization temperature, regardless of prior cold work, and SAD showed no evidence of second-phase precipitates that could be responsible for changes in mechanical properties (Fig. 11). Similar to cold-worked and aged MP35N wires, the microstructure of as-drawn and aged MP35N rods includes thin plate-like features that were identified as deformation twins, high area fractions of stacking faults, and dislocations. The aging process did not change the density of these microstructural features. These observations are consistent with a previous study by Singh and Doherty [8].

Scanning transmission electron microscopy (STEM) was utilized for its range of analytical capabilities such as composition-sensitive high-angle annular dark-field (HAADF) imaging, energy dispersive X-ray spectroscopy (EDS) and electron energy loss spectroscopy (EELS). BF-STEM images of as-drawn and aged MP35N rodstock following aging at 600 °C for 30 min showed deformation twinning and characteristic stacking fault fringes similar to those observed in conventional TEM images. HAADF-STEM images revealed bright contrast localized at stacking faults and deformation twins (Fig. 12) that can be attributed to alloying elements with the highest atomic number $Z$ [21]. Mo ($Z_{Mo} = 42$), which is present in MP35N alloys in considerable amounts (see Table 2), has an atomic number drastically higher than those of Cr ($Z_{Cr} = 24$), Co ($Z_{Co} = 27$) or Ni ($Z_{Ni} = 28$), making it the element most likely to be observed segregating to stacking faults and deformation twins. Quantitative analysis of the HAADF-STEM images for evaluation of the Mo increase at stacking faults and deformation twins is limited due to lack of details of specimen thickness, thickness of surface amorphous layer and introduced local crystal strain [22–24].

EDS measurements were performed to characterize the composition of the bright lines observed in these HAADF-STEM images. High concentrations of Mo at the stacking faults and deformation twins compared to the surrounding areas were observed. While areas around the stacking fault and deformation twin maintain an Mo concentration of about $9.9 \pm 0.7$ wt.%, as was expected, the actual fault and twins contain $12.6 \pm 0.9$ and $13.8 \pm 1.2$ wt.% Mo, which is about 25–40% higher than the matrix as shown in Fig. 13. It also showed that with

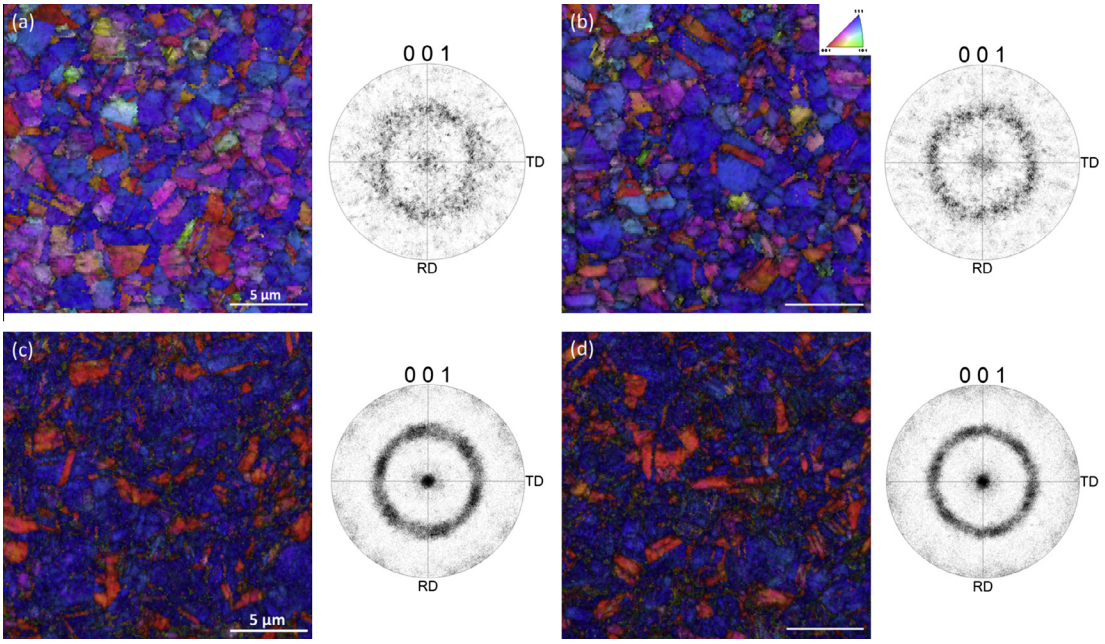


Fig. 6. Image quality with overlaid orientation image maps of MP35N wires. Corresponding pole figures are shown on the right. 37% prior cold work (sample A) wires followed by thermal treatment: (a) as drawn and (b) 700 °C for 60 s. 60% prior cold work (sample B) wires followed by thermal treatment: (c) as-drawn and (d) 700 °C for 60 s. All images are recorded in the transverse wire direction.

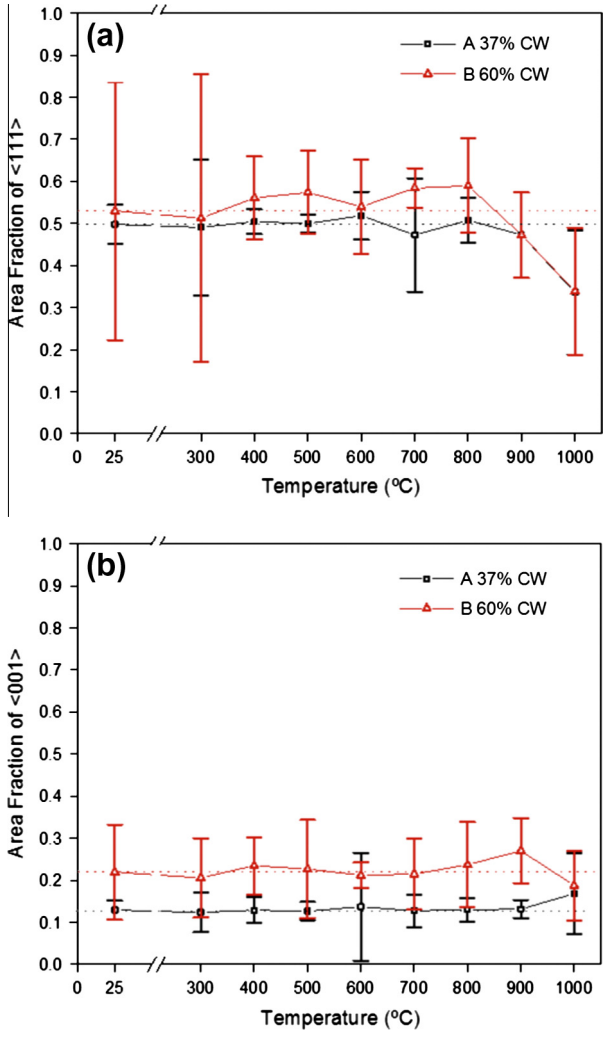


Fig. 7. Area fractions of the (a) ⟨1 1 1⟩ and (b) ⟨0 0 1⟩ texture components in MP35N wire samples A and B as a function of aging temperature. The error bars correspond to a 95% confidence level.

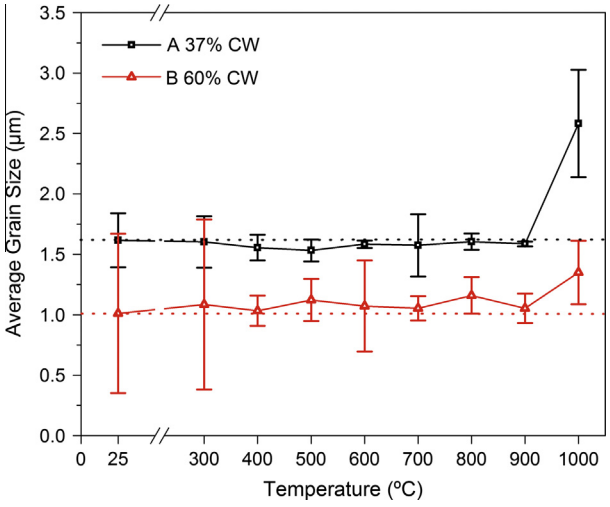


Fig. 8. Average grain size as a function of aging temperature in MP35N wires. The error bars correspond to a 95% confidence level.

an increase in Mo concentration at the stacking faults and deformation twins, a reduction in Ni and Co can also be expected. The results agree with the hypothesis of Suzuki segregation suggested by Singh and Doherty [8] and Asgari et al. [9]. Interestingly, no visible changes in the local concentration of Cr were observed near stacking faults or deformation twins.

Energy-filtered (EF) TEM was also performed to confirm the EDS observations of preferential segregation of Mo at stacking faults and deformation twins. Sample D aged at 600 °C for 30 min was used for this experiment. Since the Mo $M_{4,5}$ edge EELS signal has a delayed peak and is relatively featureless, the Ni and Co $L_{2,3}$ edges were used for energy filtering [25]. The results are presented in Fig. 14. As can be seen, the zero-loss EF-TEM image contains regions of low contrast that correspond to deformation twins. It also shows that the intensity of the combined Ni and Co $L_{2,3}$ edges was reduced at the twins by about 5–10% and was slightly higher in adjacent regions. This is consistent with EDS observations of Mo increase coupled with Ni and Co concentrations decreasing at the stacking faults and deformation twins.

## 4. Discussion

While mechanical tests can be used to measure the change in yield stress, ultimate elongation, ductility, and elastic modulus, understanding the mechanisms responsible for the secondary hardening phenomena in MP35N after aging at elevated temperatures requires an understanding of the changes in the microstructure. EBSD measurements showed that the area fractions of the major texture components and average grain sizes remained unchanged after aging of the specimens until the onset of recrystallization. A study using conventional TEM found no indications of $Co_3Mo$ precipitates or hcp martensite as suggested previously [6–8]. While formation of twins, faults and hcp platelets could in principal increase the strength of a material through a Hall–Petch-type process, only deformation twins, stacking faults and dislocation pile-ups were observed, and there was no evidence of hcp platelets. This is consistent with investigations by Asgari et al. [9], Ishmaku and Han [10,11] and Cai et al. [12]. Since grain size did not decrease following aging, including nucleation or thickening of twins, a secondary strengthening mechanism related to the Hall–Petch effect can also be ruled out.

STEM imaging and compositional analysis revealed that the local chemistry changes at stacking faults and microtwins while large area fractions of these defects were observed as seen in Fig. 15. The results confirm the existence of Suzuki segregation [26] in MP35N as hypothesized by Singh and Doherty [8] and Asgari et al. for the mechanism of secondary hardening [9]. Such preferential segregation of solute atoms to stacking faults and twins has been experimentally shown for other alloys, such as MP159 [27]. The results of electron diffraction investigations

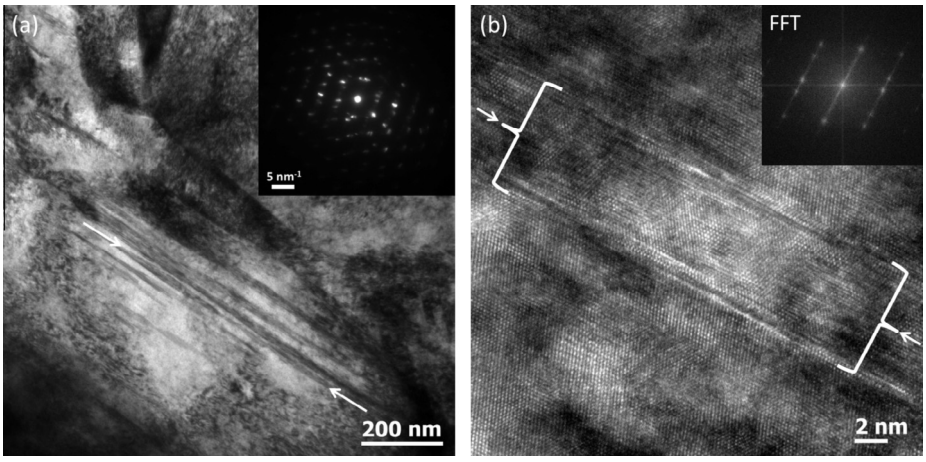


Fig. 9. (a) Low-magnification and (b) high-magnification BF-TEM images of deformation twins in MP35N wire with 37% prior cold work (sample A) aged at 700 °C for 60 s. The inset in (a) is an SAD pattern obtained from the sample and the inset in (b) is a fast Fourier transform (FFT) of the image showing the presence of deformation twins.

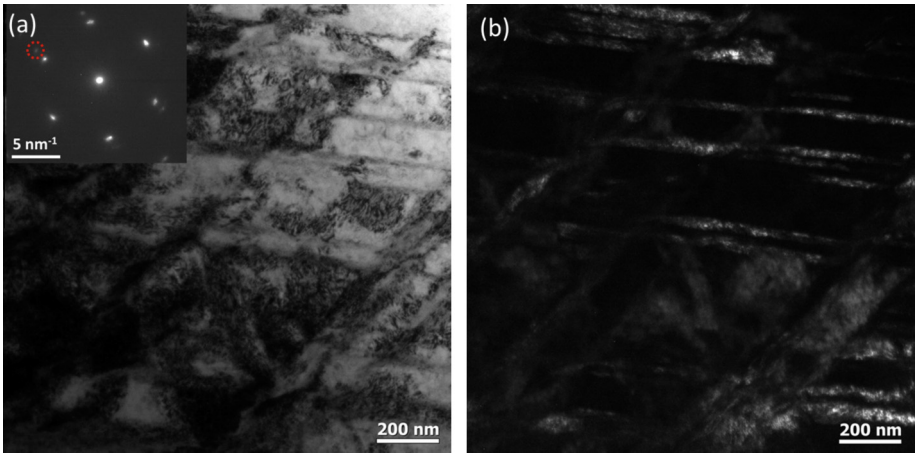


Fig. 10. (a) BF and (b) DF-TEM image pair showing deformation twins observed in MP35N rod sample D. The inset in panel (a) is the SAD pattern obtained from the area showing diffraction spots corresponding to deformation twins.

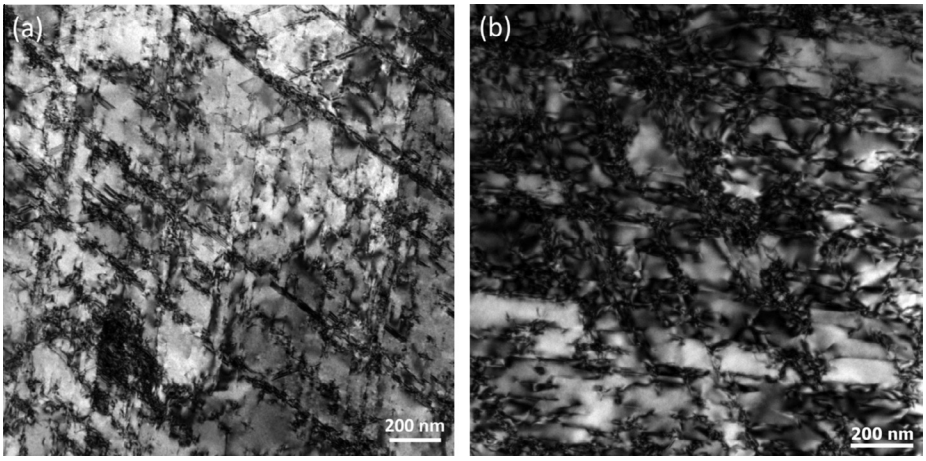


Fig. 11. BF-TEM images of (a) as-drawn MP35N rod with 25% prior cold work and (b) rodstock with 25% prior cold work and aged at 700 °C for 5 min showing the negligible effect of aging on the microstructure.

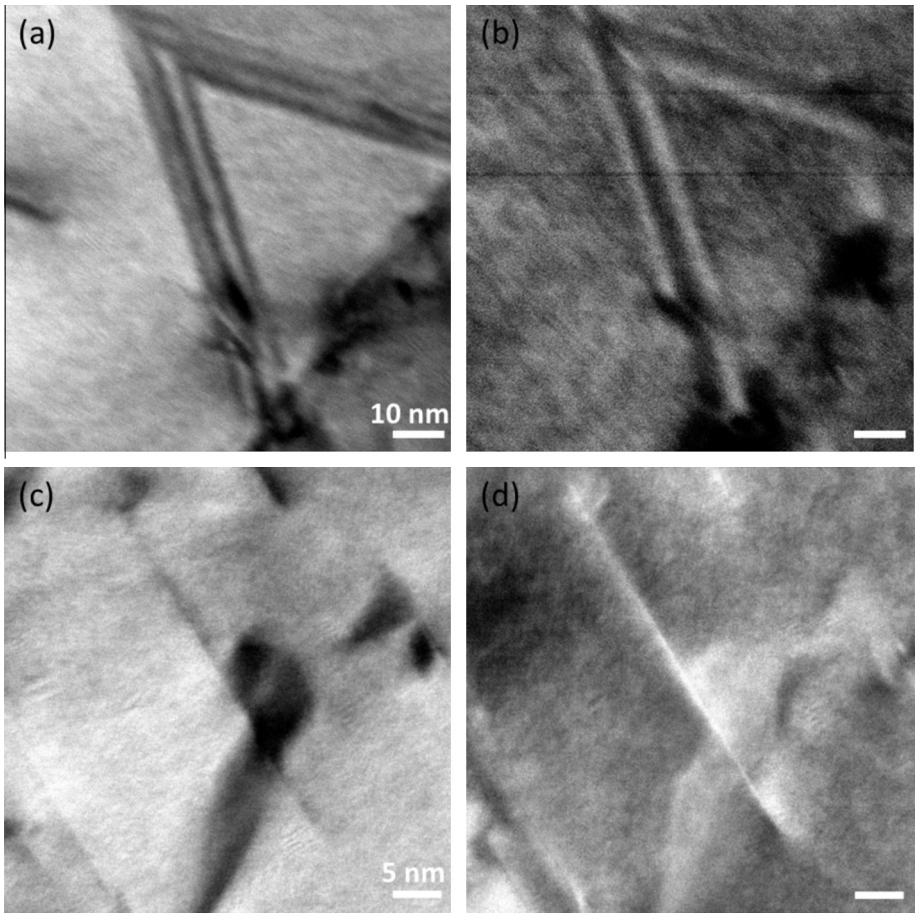


Fig. 12. (a, c) BF and (b, d) HAADF-STEM image pairs showing stacking faults in MP35N rod from samples C and D, correspondingly, aged at 600 °C for 30 min. The higher contrast in the stacking faults seen in the HAADF-STEM images indicates the presence of heavier elements.

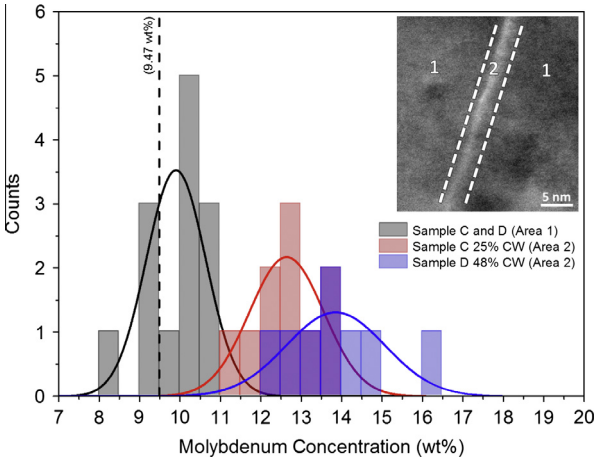


Fig. 13. Histograms of Mo concentrations at the stacking faults and deformation twins in MP35N rod (sample D). The histogram of Mo concentrations obtained from the matrix, away from faults and twins, is also shown. The inset is a HAADF-STEM image of a deformation twin with highlighted typical regions from where data for histograms are obtained.

performed in this study and synchrotron X-ray experiments [12] showed no additional phases. This suggests that segregated Mo atoms remain as a solid solution with only local concentration changes with respect to the matrix.

Typical age-hardened alloys are strengthened by second phases that nucleate and grow after precipitating from a supersaturated solid solution. MP35N does not age by precipitating out second-phase particles or nucleating hcp plates. It preferentially segregates Mo at stacking faults and twins. The minimization of free energy by adsorption of the hcp-stabilizing element Mo to stacking faults and twins, and repulsion of the fcc-stabilizing solute atoms Co and Ni to the matrix appears to be the driving force. MP35N wires are heavily deformed during cold drawing and contain large vacancy concentrations and deformation twins that assist short-range (~1 nm) self-diffusion [28]. The high concentrations of vacancies created during wire processing and the short diffusion distances could explain the rapid diffusion of Mo at elevated temperatures. It appears that the segregation of Mo at stacking faults and twins increases dislocation barriers, resulting in an increase in strength and a reduction in the ductility of aged MP35N.

## 5. Conclusions

After performing systematic mechanical tests and atomic-resolution characterization it is observed that a

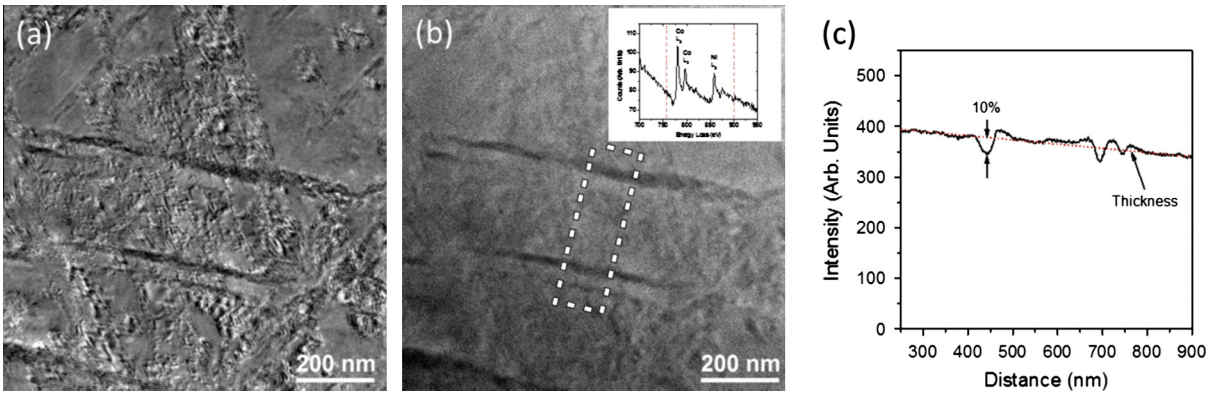


Fig. 14. EF-TEM images of MP35N with 48% cold work, aged at 600 °C for 30 min (sample D) obtained using (a) zero-loss and (b) core-loss with 755–890 eV energy window containing Co and Ni $L_{2,3}$ edges. The inset in (b) is the core-loss window used in (b). (c) The intensity of the combined Co and Ni $L_{2,3}$ edge EELS edges computed from the rectangular area shown in panel (b). The overall intensity reduction due to specimen thickness is indicated by the red dotted line. (For interpretation of the references to color in this figure legend, the reader is referred to the web version of this article.)

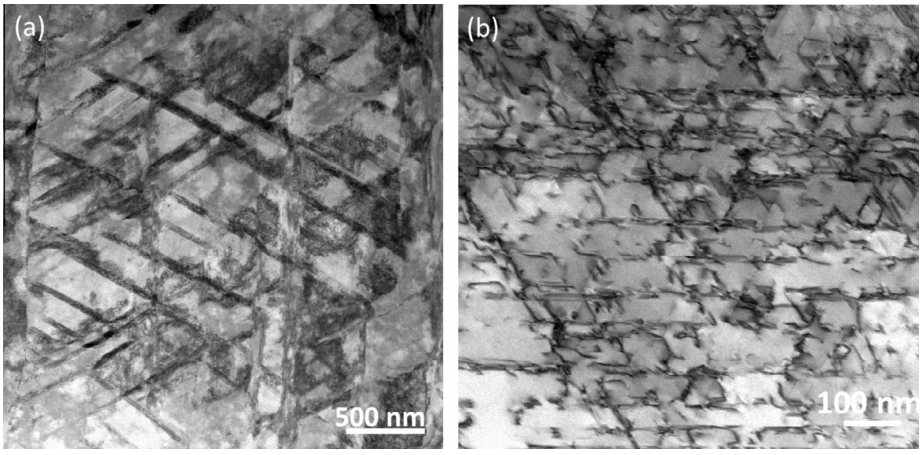


Fig. 15. Low-magnification BF-STEM images showing high area fractions of stacking faults in (a) 25% cold-worked MP35N rod aged for 30 min at 600 °C (sample C) and deformation twins in (b) 48% cold-worked MP35N rod aged for 30 min at 600 °C (sample D).

brief exposure to elevated temperatures increased the ultimate tensile strength and yield stress while decreasing the elongation of MP35N wires. Following cold drawing, the elastic modulus of MP35N decreased from 234 GPa to approximately 175 GPa. Upon aging at temperatures from 300 to 900 °C the elastic modulus increased although no changes in crystallographic orientation were observed. The grain size and major texture components do not change during aging until the onset of recrystallization. The microstructure of MP35N was found to consist of deformation twins and stacking faults, and the area fractions of these defects did not change following aging. TEM/STEM SAD and BF/DF imaging did not show formation of any second phases including hcp martensite. STEM characterization showed that Mo segregated at twins and stacking faults. Mo concentrations at stacking faults were found to be proportional to the amount of prior cold work, which agrees with the degree of strengthening observed during tension testing.

## Acknowledgements

The authors would like to acknowledge the Medtronic Neuromodulation leadership for financial support of this research. D.S. would also like to thank Dr. J. Schaffer of Fort Wayne Metals for helpful discussions, Dr. O. Ugurlu and Dr. J. Myers for helpful discussions and assistance with TEM, and Ms. M. Bush of Medtronic for careful proofreading of this manuscript. Parts of this work were carried out at the Characterization Facility of the University of Minnesota, which receives partial support from NSF through the MRSEC program. Parts of this work were carried out at the University of Minnesota Nano Center, which receives partial support from NSF through the NNIN program.

## References

[1] Smith GS. US patent no. 3,356,542.

[2] Escalas F, Galante J, Rostoker W, Coogan PH. J Biomed Mater Res 1975;9(3):303–13.
[3] Altman PA, Meagher JM, Walsh DW, Hoffmann DA. J. Biomed Mater Res 1998;43(1):21–37.
[4] Schaffer JE. MS thesis. Purdue University; 2007.
[5] Graham A, Youngblood J. Metall Mater Trans B 1970;1(2):423–30.
[6] Drapier JM et al. Cobalt 1970;49:171–86.
[7] Raghavan M, Berkowitz BJ, Kane RD. Metall Mater Trans A 1980;11A:203–7.
[8] Singh R, Doherty R. Metall Mater Trans A 1992;23(1):307–19.
[9] Asgari S et al. Acta Mater 1998;46(16):5795–806.
[10] Ishmaku A, Han K. Mater Charact 2001;47:139–48.
[11] Ishmaku A, Han K. J Mater Sci 2004;39:5417–20.
[12] Cai S, Barrow A, Yang R, Kay L. Biomaterials science: processing, properties, and applications III. Ceram Trans 2013;242:19.
[13] VanderVoort GF Geertruyden WV. <http://www.georgevander-voort.com/met_papers/EBSD/EBSD_Specimen_Prep_Paper.pdf>.
[14] Bher MJ, Mkhoyan KA, Aydil ES. ACS Nano 2010;4:5087–94.
[15] Li BQ, Sorensen D, Steigauf T. Medical device materials VI: proceedings from the materials & processes for medical devices conference 2011. Materials Park, OH: ASM International; 2013. p. 131.
[16] Shaji M, Kalidindi R, Doherty R. Mater Sci Eng A 1999;272:371–9.
[17] http://www.fwmetals.com/mp35n-superalloy.php.
[18] Otomo T, Matsumoto H, Nomura N, Chiba A. Mater Trans 2010;51(3):434–41.
[19] Benito JA, Manero JM, Jorba J, Roca A. Metall Mater Trans A 2005;36:3317–24.
[20] Li B, Steigauf T, McIntyre P, Sorensen D. Medical device materials V: proceedings from the materials & processes for medical devices conference 2009. Materials Park, OH: ASM International; 2010. p. 111–4.
[21] Pennycook SJ, Boatner LA. Nature 1988;336:565–7.
[22] Mkhoyan KA, Maccagnano-Zacher SE, Kirkland EJ, Silcox J. Ultramicroscopy 2008;108:791.
[23] Muller DA, Nakagawa N, Ohomoto A, Grazul JL, Hwang HY. Nature 2004;430:657.
[24] Jeong JS, Ambwani P, Jalan B, Leighton C, Mkhoyan KA. ACS Nano 2013;7:4487.
[25] Ahn CC, Krivanek OL. EELS atlas. Gatan Inc.; 1988.
[26] Suzuki H. Dislocations and mechanical properties of crystals. General Electric Company; 1957. p. 368–73.
[27] Han GW, Jones IP, Smallman RE. Acta Mater 2003;51:2731–42.
[28] Seeger A. Philos Mag Lett 2007;87(2):95–102.